Eur Biophys J (2004) 33: 59–67
DOI 10.1007/s00249-003-0343-6

ARTICLE

**Károly Módos · Rita Galántai · Irén Bárdos-Nagy
Malte Wachsmuth · Katalin Tóth · Judit Fidy
Jörg Langowski**

Maximum-entropy decomposition of fluorescence correlation spectroscopy data: application to liposome–human serum albumin association

Received: 25 February 2003 / Revised: 25 April 2003 / Accepted: 25 April 2003 / Published online: 30 August 2003

Abstract Fluorescence correlation spectroscopy was used to measure the diffusion behavior of a mixture of DMPC or DMPC/DMPG liposomes with human serum albumin (HSA) and mesoporphyrin (MP), which was used as the fluorescent label for liposomes and HSA as well. For decomposing the fluorescence intensity autocorrelation function (ACF) into components corresponding to a liposome population, HSA and MP, we used a maximum entropy procedure that computes a distribution of diffusion times consistent with the ACF data. We found that a simple parametric non-linear fit with a discrete set of decay components did not converge to a stable parameter set. The distribution calculated with the maximum entropy method was stable and the average size of the particles calculated from the effective diffusion time was in good agreement with the data determined using the discrete-component fit.

Keywords Fluorescence correlation spectroscopy · Human serum albumin · Liposomes · Maximum entropy data analysis · Mesoporphyrin

Introduction

Fluorescence correlation spectroscopy (FCS) was introduced about 30 years ago (Elson and Magde 1974; Magde et al. 1972, 1974) as a method to analyze fluorescence intensity fluctuations from a small laser-illuminated volume. The temporal behavior of the fluorescence intensity is characterized by its normalized autocorrelation function (ACF). In a typical FCS experiment, molecules free in solution move through the observation volume by Brownian motion, generating fluorescence fluctuations. Binding to a ligand slows down the molecules and increases the typical dwell time in the observation volume. The average number of molecules of free and bound species and the respective diffusion coefficients can be recovered from the ACF. Numerous other sources of fluctuations can be studied with FCS (Chen et al. 2000 and references therein). The implementation of confocal microscopy for FCS (Qian and Elson 1991; Rigler et al. 1993) increases the sensitivity, improves the spatial resolution, and reduces the observation volume well below 1 fL, corresponding to only a few fluorescent molecules at nanomolar concentrations. FCS is also becoming increasingly important in the characterization of biological macromolecules and their interactions. Its high sensitivity, the low concentrations used in the measurement, and the very small observed volume offer a very effective method to observe and characterize molecules inside living cells: observing the behavior of the molecules in different parts of the cell can yield information about the environment of these molecules.

The FCS experiments to which we applied the maximum entropy analysis here were originally planned to characterize the interaction between human serum albumin (HSA), mesoporphyrin, and two kinds of liposome compositions. In systems consisting of HSA, differently charged small unilamellar vesicles (SUV), and mesoporphyrin (MP), steady-state and time-resolved fluorescence measurements and differential scanning calorimetry experiments had suggested an interaction between HSA and liposomes (Bárdos-Nagy et al. 1998; Galantai and Bardos-Nagy 2000; Galantai et al. 2000). Before embarking on a detailed study of that interaction, which will be published separately, this paper aims at studying the application of the maximum entropy method to FCS data containing a distribution of diffusing components. As a model we used neutral (1,2-dimyristoyl-*sn*-glycero-3-phosphatidylcholine,

M. Wachsmuth · K. Tóth · J. Langowski (✉)
Division of Biophysics of Macromolecules (H0500),
Deutsches Krebsforschungszentrum,
Im Neuenheimer Feld 280,
69120 Heidelberg, Germany
E-mail: jl@dkfz-heidelberg.de

K. Módos · R. Galántai · I. Bárdos-Nagy · J. Fidy
Department of Biophysics and Radiation Biology,
Semmelweis University, Puskin utca 9,
1088 Budapest, Hungary

DMPC) and negatively charged [19:1 w/w% of DMPC and 1,2-dimyristoyl-*sn*-glycero-3-phosphatidylglycerol (DMPC/DMPG)] SUV liposomes. Since MP binds reversibly to HSA ($K_a = 2.5\times 10^7$ M^{-1}) and also to the liposomes [$K_L = (1.5–4)\times 10^4$ M^{-1}, depending on the lipid components of the liposomes], we assumed that—at a sufficient excess of HSA or liposomes—we could follow their diffusion through the fluorescent signal of MP. Utilizing the size difference of HSA and liposomes, and the distinct binding affinity of MP to them, the formation of the HSA–liposome complexes was observed by MP-labelled HSA.

Materials and methods

Chemicals

The samples were prepared in 10 mM sodium phosphate buffer at pH 7.4. The DMPG, DMPC, 1×crystallized and lyophilized HSA, and MP dihydrochloride were purchased from Sigma. All solvents [chloroform, methanol, ethanol, dimethylformamide (DMF)] were obtained from Merck. The chemical components in the samples were of spectroscopic purity. Sephadex G100 Superfine, used to purify HSA, was purchased from Pharmacia Fine Chemicals.

Preparation of porphyrin solution

A stock solution of MP was prepared in DMF and kept in the dark to avoid photodamage. For the measurements, solutions were prepared by diluting with pH 7.4 phosphate buffer and used immediately after preparation. The concentration of porphyrin solutions was determined by using the Soret band absorbance of the dye. The molar extinction coefficient for MP dissolved in DMF, $\epsilon_{399} = 1.55\times 10^5$ M^{-1} cm^{-1}, was determined by ourselves and used in later calculations.

Preparation of HSA solution

HSA was purified by gel filtration (Sephadex G100 column equilibrated with 10 mM phosphate buffer at pH 7.4) and characterized by SDS gel electrophoresis. The purified fractions were lyophilized and stored at −20 °C. The concentration of HSA solutions was determined spectrophotometrically (Reddi et al. 1981).

Preparation of liposomes

Stock solutions of DMPC/DMPG (19:1) and DMPC in chloroform/methanol (9:1) were dried to a film using a stream of nitrogen. Lipids were hydrated with buffer by hand-shaking followed by sonication (MSE Desintegrator P 6/527) until no further decrease of turbidity could be detected. The samples were centrifuged (Beckman J2-21 centrifuge, 19,000 rpm, 45 min) to eliminate remnants of multilamellar vesicles as well as metal particles from the sonicator. The phospholipid content of the liposome suspensions was quantified according to Rouser et al. (1969). For calculations and graphic representations, the molar lipid concentration was used instead of the liposome concentration in all cases when liposomes were used. For calculating molar liposome concentrations, the liposome size distributions were assumed to be the same as in our previous work under these conditions (Galantai et al. 2000).

FCS experiments

FCS measurements were performed in an apparatus of our own construction (Langowski and Tewes 2000). It consists of a module containing the confocal optics, which connects to the video port of an inverted microscope (Olympus IX-70). The laser (Omnichrome 20 mW Ar-Kr laser) is coupled into the module via fiber optics. The observation lens was an Olympus 60×/1.2W water immersion type with cover slip correction. For the experiments described here, an excitation wavelength of 488 nm was selected via a filter and a dichroic mirror in the FCS module. The fluorescence was detected after separation through a dichroic mirror (505DRLP) and filter (LC 635DF55 for porphyrin or LC 530DF30 for Alexa 488) (Omega Optical, Brattleboro, USA) by avalanche photon diode detectors (Perkin-Elmer single-photon counting module SPCM-AQ 141). Autocorrelation functions were collected from the photon stream by an ALV-5000 correlator card and ALV correlator software (ALV, Langen, Germany). The experiments were typically performed at a laser power of 2 μW, corresponding to a power density (in a focus of 0.15 μm radius) of 2.8 kW/cm^2. Autocorrelation functions were accumulated in five blocks of 60 s each.

FCS theory and data analysis

Overview of FCS theory

The primary data obtained in an FCS measurement is the time-dependent fluorescence intensity, $F(t)$, which is proportional to the number of particles in the observation volume at time t. The autocorrelation function of $F(t)$ contains all the relevant information relating to the diffusion of the fluorophores. The normalized autocorrelation function $G(\tau)$ is computed as:

$$G(\tau) = \frac{\langle F(t)F(t+\tau)\rangle}{\langle F(t)\rangle^2} \tag{1}$$

For obtaining quantities such as diffusion coefficients, concentrations, or reaction rate constants, one has to fit a theoretical correlation function to the measured $G(\tau)$ which is based on a model that contains these quantities as free parameters. For a solution of a single fluorescent species with diffusion coefficient D and molar concentration c and for Gaussian profiles for the excitation intensity and detection efficiency, $G(\tau)$ evaluates to (Rigler et al. 1993):

$$G(\tau) = \frac{1}{cV_{\text{eff}}}\left(1+\frac{4D\tau}{w_0^2}\right)^{-1}\left(1+\frac{4D\tau}{z_0^2}\right)^{-1/2} + 1 \tag{2}$$

Here, V_{eff} is the effective observation volume, which depends on the geometry of the focus for excitation and emission, w_0 and z_0 are the half-widths of the focus in the x–y plane (the observation plane of the lens), and in the z-direction, respectively.

V_{eff}, w_0, and z_0 can be measured independently by calibration with a solution of a fluorophore of known concentration and diffusion coefficient. If only relative changes are of interest, one can use the average particle number, $N = cV_{\text{eff}}$, and an effective diffusion time, $\tau_{\text{diff}} = w_0^2/4D$, as parameters:

$$G(\tau) = 1N\left(1+\frac{\tau}{\tau_{\text{diff}}}\right)^{-1}\left(1+\frac{\tau}{\tau_{\text{diff}}\kappa^2}\right)^{-1/2} + 1 \tag{3}$$

where κ (also called the structure factor) is the axial ratio of the observation volume, z_0/w_0.

For a high-aperture lens (NA = 1.2) at optimal alignment, κ typically ranges between 4 and 6. In a typical FCS experiment, one determines κ on a monodisperse solution of a known fluorophore and keeps its value fixed for the measurements of the unknown sample.

In a mixture of molecules with different diffusion coefficients, the fluorescence intensity autocorrelation function is a sum of the contributions of the individual species. The general form of $G(\tau)$ for a mixture of m different fluorescent species with diffusion times $\tau_{\mathrm{diff},i}$ is then given by:

$$G(\tau) = \frac{1}{N}\sum_{i=1}^{m} \rho_i g_i\left(\tau, \tau_{\mathrm{diff},i}\right) + 1 \tag{4}$$

with:

$$g_i\left(\tau, \tau_{\mathrm{diff},i}\right) = \left(1 + \tau/\tau_{\mathrm{diff},i}\right)^{-1}\left(1 + \tau/\left(\tau_{\mathrm{diff},i}\cdot\kappa^2\right)\right)^{-1/2} \tag{5}$$

The ρ_i are the relative amplitudes corresponding to molecules with distinct diffusion coefficients; they are related to their concentrations c_i by:

$$\rho_i = \frac{\phi_i^2 c_i}{\sum_{i=1}^{m} \phi_i^2 c_i} \tag{6}$$

where ϕ_i is the quantum yield of species i.

Up to Eq. (4), only number fluctuations in the detection volume were considered to contribute to the fluctuations of the light intensity at the detector, under the simplifying assumption that an excited fluorophore will emit a constant light flux. Because of the quantum nature of light and the photophysics of fluorescent molecules, this is not the case. The most important effect that has to be considered is a transition of the excited molecule into the triplet state. This will "interrupt" the stream of photons for approximately the triplet lifetime of the fluorophore and add another contribution to the autocorrelation function, which—in good approximation—is (Widengren et al. 1995):

$$G(\tau) = \left(1 + \beta e^{-\lambda\tau}\right)\frac{1}{N}\sum_{i=1}^{m} \rho_i g_i\left(\tau, \tau_{\mathrm{diff},i}\right) + 1 \tag{7}$$

The amplitude of the triplet term β and its relaxation rate λ increase with the excitation light intensity up to a limit given by the excitation, emission, and intersystem crossing probabilities of the fluorophore.

FCS data analysis

For analyzing FCS data from samples of biological macromolecules, Eq. (7) is often applied since it is known a priori that the system contains a small number of discrete components (for example, in a protein–protein or protein–DNA interaction). Thus, FCS autocorrelation functions were first analyzed by QUICKFIT, a fitting program developed in our group under the application framework Delphi (Borland, Scotts Valley, USA) and running on a PC under Windows. The software is based on the Levenberg–Marquardt algorithm for non-linear least-squares multi-parameter curve fitting (Press et al. 1986) and allows the automatic analysis of a set of ACFs, fitting the amplitude and decay time of up to three diffusing components and up to two non-fluorescent contributions, as well as the baseline and the structure factor. The parameters describing the non-fluorescent contribution were then used in the further analysis by the maximum entropy procedure.

We shall demonstrate in the following that for biological samples which are intrinsically polydisperse, such as liposomes, protein aggregates, or intracellular fluorescent components, a discrete component fit often yields uninterpretable results because the number of parameters necessary for a good fit exceeds the information content of the experiment. In such a case, a distribution of decay functions should be fitted to the data, which can be characterized by a small number of independent parameters (such as width, area, and first moment).

In that case, the sum in Eq. (7) is approximated by an integral over the diffusion time τ_{diff}, and the amplitudes of the components, ρ_i, by the desired normalized distribution $\rho(\tau_{\mathrm{diff}})$:

$$G(\tau) = \left(1 + \beta e^{-\lambda\tau}\right)\left(\frac{1}{N}\int_{\tau_{\min}}^{\tau_{\max}} \rho(\tau_{\mathrm{diff}})\, g(\tau, \tau_{\mathrm{diff}})\mathrm{d}\tau_{\mathrm{diff}}\right) + 1 \tag{8}$$

The task is then to find the inversion of the integral transformation in Eq. (8), obtaining the distribution $\rho(\tau_{\mathrm{diff}})$ from a measured noisy data set $G(\tau)$. Inversion problems of this kind are known to be ill-posed, that is, an infinite number of solutions compatible with experimental (or numerical) noise exists, which may deviate infinitely from each other. The distribution $\rho(\tau_{\mathrm{diff}})$ in Eq. (8) is positive additive, i.e. negative values are not allowed and the transformation of a sum of distributions is equal to the sum of the transformations of the individual components. For finding such a distribution function that is physically "reasonable" and compatible with the data, a variety of regularization methods exist.

The "maximum entropy" method (MEM) has been used to solve this and other problems involving inverse integral transformations (Gull and Daniell 1978; Skilling and Bryan 1984). Here, the entropy of the distribution $\rho(\tau_{\mathrm{diff}})$ is defined as:

$$S = -\sum_{i=1}^{N} \rho\left(\tau_{\mathrm{diff},i}\right) \ln \rho\left(\tau_{\mathrm{diff},i}\right) \tag{9}$$

where N is the number of discrete values of τ_{diff} through which the distribution is determined. Given two solutions of equal merit (e.g., in terms of their least-squares fits to the data), the solution with the larger entropy extracts the most information out of the original data without making unreasonable assumptions about unavailable information.

MEM analysis maximizes the posterior probability of a particular model [here the distribution function $\rho(\tau_{\mathrm{diff}})$], given a measured data set [here $G(\tau)$], by maximizing the parameter $Q = \alpha S - L$. Here, L is the likelihood of the fit, given by the sum of the squared deviations of the model points from the data (M points), normalized by their variance:

$$L = \frac{1}{2}\sum_{j=1}^{M} \left(G_{\mathrm{theo}}\left(\tau_j\right) - G_{\exp}\left(\tau_j\right)\right)^2 \Big/ \sigma_j^2 \tag{10}$$

and α is a regularization parameter that controls the relative influence of the entropy and likelihood on the fit. Higher values of α will lead to smoother distributions, while for small α values the distribution will contain features that are due to random noise in the data. The correct choice of α can be determined by a criterion based on Bayesian probability theory, as shown by Bryan (1990).

Several years ago, Bryan (1990) and Langowski and Bryan (1991) proposed an MEM procedure that was particularly well adapted to oversampled data, such as small-angle scattering data or multiexponential decays obtained in fluorescence decay or dynamic light scattering. In such data sets, the number of independent pieces of information in the data is much smaller than the number of data points. It was shown there that the MEM fitting procedure can be greatly accelerated for oversampled data by representing the distribution function $\rho(\tau_{\mathrm{diff}})$ by a set of linearly independent basis functions.

Let the distribution be related to the measured data through a linear transformation:

$$\mathbf{d} = \mathbf{T}\mathbf{f} \tag{11}$$

where $\mathbf{d}$ is an M-element vector containing the autocorrelation function $G(\tau_i)$, $\mathbf{f}$ is an N-element vector containing the distribution $\rho(\tau_{\mathrm{diff},j})$, and $\mathbf{T}$ is a transformation matrix whose elements are given in our case by the values of Eq. (5) for all pairs of (τ_i, $\tau_{\mathrm{diff},j}$):

$$T_{ij} = g\left(\tau_i, \tau_{\mathrm{diff},j}\right) \tag{12}$$

In previous work (Bryan 1990), a non-linear solution of this problem in the singular value space of $\mathbf{T}$ was described which greatly improved the convergence and stability of the fitting procedure. In those papers, special solutions were described for dynamic light scattering data and Fourier transformation.

In the case of FCS, the distribution in its discretized form is given by the coefficients ρ_j, and the data vector is the measured correlation function $G(\tau_i)$. The transformation matrix elements are given by Eq. (12). Application of the maximum entropy algorithm described by Bryan (1990), however, is complicated by the presence of the $(1+\beta e^{-\lambda\tau})$ term in Eq. (8), which in itself is τ-dependent. To overcome this difficulty, we have chosen to determine the parameters β and λ from a separate discrete fit first, before applying the MEM algorithm.

Results and discussion

The rationale for using MP as a non-covalent fluorescent label for both HSA and liposomes is based on our previous work on the physicochemical properties of this system (Galantai et al. 2000). We found that the bound porphyrin could be easily detected in our FCS setup and gave a well-defined correlation signal for HSA, liposomes, and the HSA–liposome mixtures; on the other hand, the free porphyrin dye is hardly detectable [which is in agreement with the increase of fluorescence intensity of MP after binding HSA or liposomes (Bárdos-Nagy et al. 1998)]. We therefore used Alexa 488 as a standard for a small dye molecule.

As a first experiment, we characterized the diffusion of MP-tagged liposomes and the MP–HSA complex under conditions of a large molar excess of lipid or protein over the label. The MP concentration was 5×10^{-9} M, HSA was at 10^{-6} M, and the total lipid concentration was 10^{-3} M. Two types of liposomes were used, as described in the Methods section: one prepared from 100% DMPC, the other from a 19:1 w/w% DMPC/DMPG mixture. From the known size distribution of the liposomes under these preparation conditions and the known surface area per lipid molecule (Galantai et al. 2000), we estimate a liposome concentration of 2×10^{-8} M. The average diameter for this type of preparation was 75 nm for the DMPC liposomes and 50 nm for the DMPC/DMPG liposomes (Galantai et al. 2000).

Figure 1 (lower panel) shows typical autocorrelation functions (ACF) of the basic components under these conditions. Figure 1 (upper panel) gives the ACF of Alexa 488 as a control for a monodisperse system. The Alexa data are used to calibrate the τ scale and to calculate the diffusion constant of the particles.

We obtained stable values for the diffusion constant, the amplitude, and the non-fluorescent term of Alexa 488 using a non-linear least-squares fit with discrete components. The translational diffusion constant of Alexa 488 was determined by comparing its diffusion time with that of rhodamine 6G, with known diffusion coefficient. Here, we measured $\tau_{\mathrm{diff}}=52$ µs for Alexa 488 with excitation at 488 nm and detection at 515–545 nm, and $\tau_{\mathrm{diff}}=70$ µs for rhodamine 6G with excitation at 568 nm and detection at 608–662 nm. Correcting for the wavelength-dependent dimensions of the focal volume and using $D_t=2.8\times10^{-10}$ m^2 s^{-1} for rhodamine 6G (Rigler et al. 1993), this yields a value of $D_t=2.4\times10^{-10}$ m^2 s^{-1} at room temperature for Alexa 488. The decay curves for the HSA–MP mixture could be fitted with one or two discrete fluorescent components; however, the two-component analysis did not result in a significantly improved fit, as judged by the χ^2 value. Table 1 presents the results of the discrete fit at 25 °C. The diffusion constant of HSA, as determined from the one-component fit in Table 1, is in good agreement with the value of 6.0×10^{-11} m^2 s^{-1} as measured by Oncley et al. (1947) at room temperature, and with the value of 6.27×10^{-11} m^2 s^{-1} determined by Ferrer et al. (2001).

The liposome data from Fig. 1 were also first analyzed with the discrete-component model. Here we found that the fit became very unstable: the fitted parameters exhibited large variations between different measurements on the same sample and for different starting values of the fit parameters on the same measurements. The reasons for this were presumably both the higher noise level of the primary data and the width of the size distribution of the liposomes. Taken together, this resulted in data that could not be fitted with a small number of discrete decay components, and did not contain enough information to determine reliably the D values and amplitudes of a larger number of components. Thus, for these types of sample a method that yields a distribution of D values might be more appropriate.

Our previously described maximum entropy algorithm (MEM) (Bryan 1990) is well adapted to fitting problems such as the one described here, i.e. to data consisting of a sum of smooth decay functions. A specific feature of FCS data, which makes the application of MEM less straightforward, is the presence of the non-fluorescent decay part which constitutes the τ-dependent multiplicative term in Eq. (7). While such constant parameters can in principle be determined by a Bayesian probability criterion or integrated out of the problem [as was done for the baseline for dynamic light scattering data by Langowski and Bryan (1991)], this procedure complicates the fit and can lead to instabilities. We therefore used the discrete fit in a first step for determining the total amplitude of the correlation function, $1/N$ (where N is the number of particles in the detection volume), and the amplitude β and relaxation rate λ of the non-fluorescent part.

The result was used to calculate the elements of the transformation matrix **T**:

$$T_{i,j}=\frac{1}{N}\left(1+\beta e^{-\lambda\tau_j}\right)\frac{1}{1+\tau_j/\tau_{\mathrm{diff},i}} \tag{13}$$

where τ_j is the correlation time (discretized by the index j) and $\tau_{\mathrm{diff},i}$ is the diffusion time of the i-th component. For a measured data set **d** with $d_j=G(\tau_j)$, the most probable distribution vector **f** with $f_i=\rho(\tau_{\mathrm{diff},i})$ is then determined through maximum-entropy optimization in the singular vector space of **T**, as described by Bryan (1990).

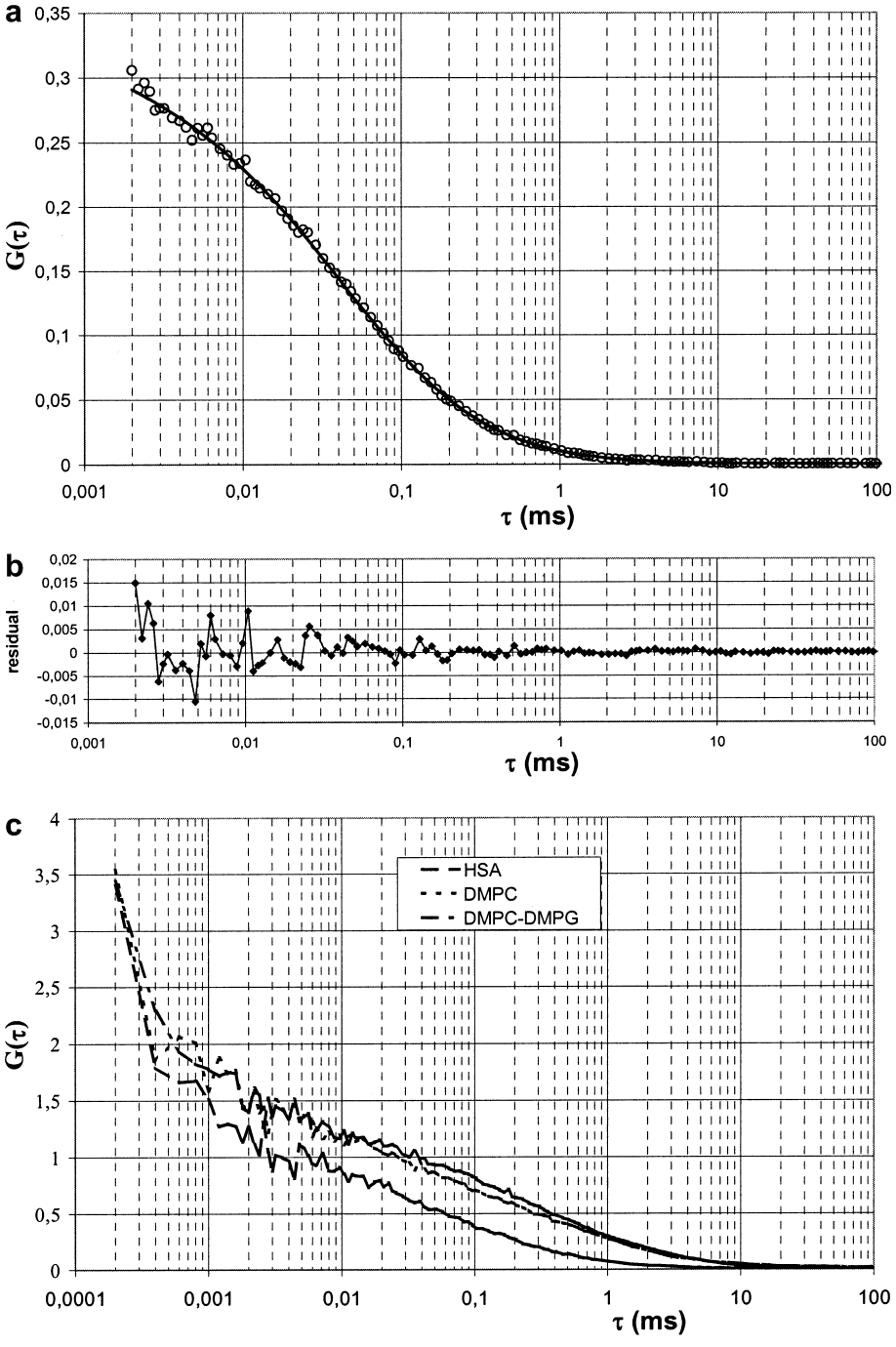

Fig. 1 (**a**) FCS autocorrelation functions of Alexa 488 used as a standard: measured data (*open circles*) and maximum entropy fit (*solid line*). (**b**) Residuals of the fit. (**c**) FCS autocorrelation functions of the lipid and protein components in the presence of MP

Figure 2 shows the distribution functions obtained from applying MEM to the Alexa and the HSA data. The Alexa sample gives a monomodal distribution with the median of the peak at 50 μs, in good agreement with the value from the discrete fit. For $\tau_{diff} < 1$ μs, the distribution curve increases again to a constant value of 0.006. This is a typical feature of the maximum-entropy fitting algorithm; for regions in which no information exists (i.e., only data for correlation times > 1 μs were used), the most probable value of the distribution function is not zero but the average over the region of τ_{diff} where experimental data exist. For a more thorough discussion of this subject in the framework of Bayesian statistics, see Bryan (1990).

Table 1 Diffusion constants of Alexa 488 and HSA at 25 °C derived from one-component fits using the discrete non-linear fitting method. Errors given are standard errors of the mean derived from three different fits

	τ_{diff} (ms)	D_t (m^2 s^{-1})
Alexa 488	0.052 ± 0.0007	$(2.4 \pm 0.03) \times 10^{-10}$
HSA	0.173 ± 0.012	$(7.2 \pm 0.5) \times 10^{-11}$

The diffusion time distribution for the FCS data from the HSA–MP mixture shows two clearly separated

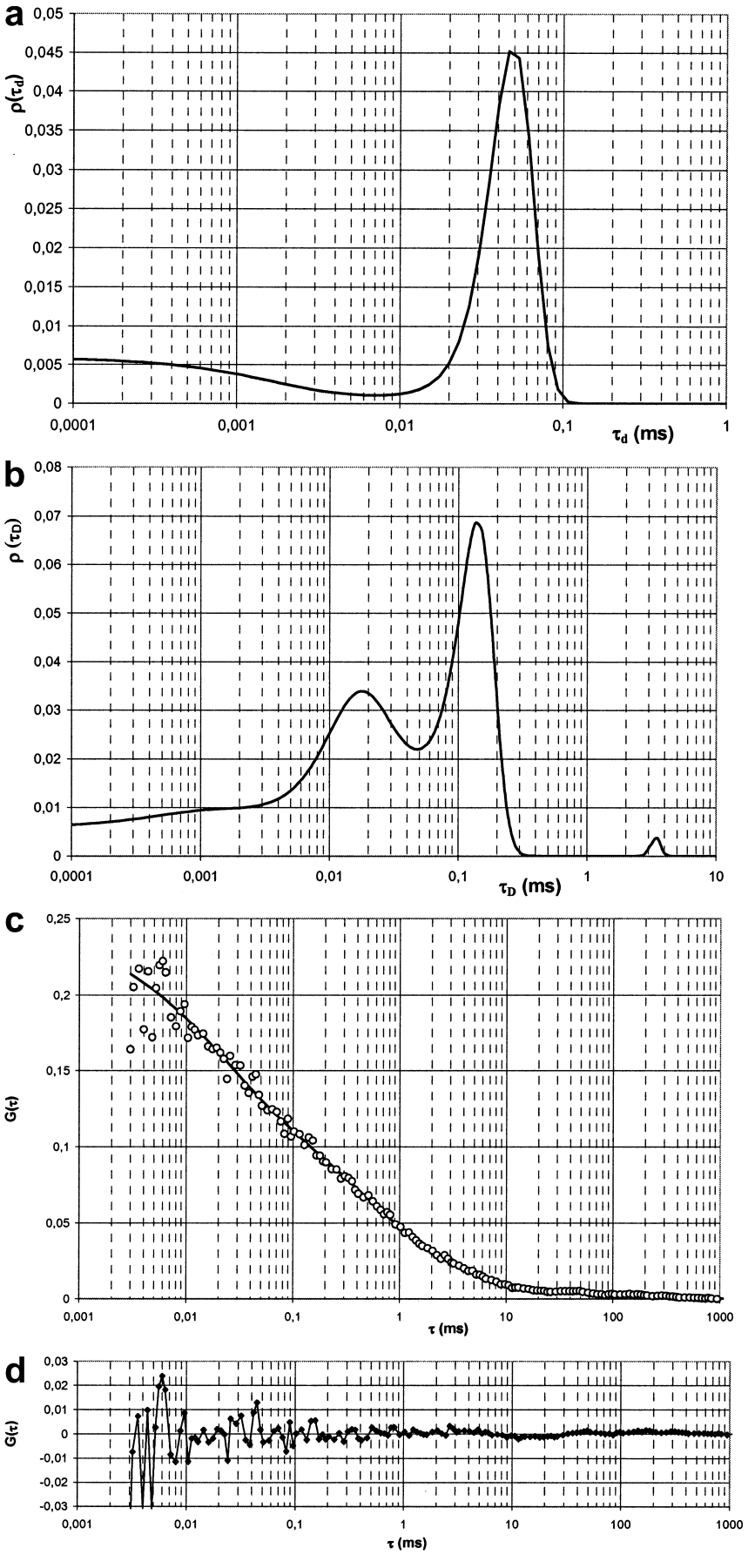

Fig. 2 FCS diffusion time distributions calculated by MEM from Alexa 488 (**a**) and HSA in the presence of MP (**b**); (**c**) MEM fit to the FCS autocorrelation function from the HSA sample in (**b**) and residuals (**d**)

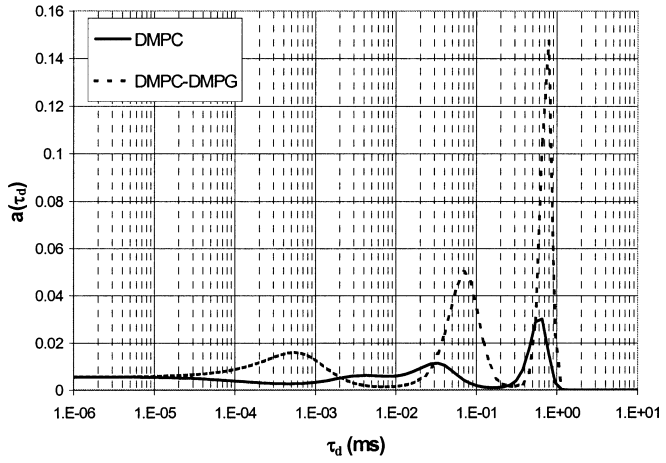

Fig. 3 Diffusion time distributions for DMPC and DMPC/DMPG liposomes in the presence of MP, as obtained from MEM fits to the FCS autocorrelation functions

components. The main peak has a median value of $\tau_{diff} = 0.15$ ms, corresponding to a diffusion coefficient of 8×10^{-11} m^2 s^{-1}, in reasonable agreement with both the one-component fit and the literature value. The second peak, at $\tau_{diff} = 18$ μs, probably originates from free MP and/or incomplete compensation of the non-fluorescent term. Since the main HSA peak was separated from this feature by an order of magnitude, we did not consider the presence of this peak an important problem in the following analysis.

The distribution curves calculated from the MEM analysis on the liposome samples are shown in Fig. 3. The peaks represent relative values normalized to a total area (correlation amplitude) of 1; for comparison, they have to be multiplied with the $1/N$ value determined separately.

A small peak at around 1 μs is present in most of the data sets; this corresponds to the non-fluorescent component, which is not eliminated entirely using the parameters estimated from the discrete fit. Through a systematic variation in the amplitude β with subsequent recalculation of the transformation matrix, this peak could probably be suppressed even more. The peak found at $\tau_{diff} < 0.1$ ms is also present in the buffer and probably originates in a slight contamination by traces of fluorescent molecules other than MP, whose quantum efficiency is rather low. The peaks corresponding to the liposomes are well separated from the small contaminant.

Given the τ_{diff} value of the Alexa 488 reference and its known diffusion coefficient D_t corrected to 32 °C, the D_t of liposomes and HSA may be computed from their τ_{diff} values (Table 2). Assuming a spherical shape for the protein and liposomes, we can also transform the diffusion coefficient into a hydrodynamic radius R_h using the Stokes–Einstein relation $D_t = k_B T/6\pi\eta R_h$, with k_B being Boltzmann's constant, T the temperature, and η the viscosity of the solvent. The results in Table 2 show that for Alexa 488 and HSA the diffusion coefficients obtained from the discrete-component fit and from the MEM procedure are in very good agreement. The hydrodynamic

Table 2 Diffusion times (measured at 32 °C), computed diffusion constants, and hydrodynamic radii for the Alexa standard and the different protein and liposome components as obtained from the MEM distributions

	τ_{diff} (ms)	D_t (m^2 s^{-1})	r (nm)
Alexa 488	0.05	2.5×10^{-10}	
HSA	0.15	9.7×10^{-11}	3
DMPC liposome	0.6	2.4×10^{-11}	12
DMPC/DMPG liposome	0.7	2.1×10^{-11}	14

Table 3 Compositions of the liposome/HSA/MP samples used in the experiments

	Lipids (mol/L)	HSA (mol/L)	MP (mol/L)
A	8.3×10^{-5}	5×10^{-7}	5×10^{-9}
B	1.7×10^{-4}	5×10^{-7}	5×10^{-9}
C	3.3×10^{-4}	5×10^{-7}	5×10^{-9}
D	8.3×10^{-4}	5×10^{-7}	5×10^{-9}

radius of the liposomes is similar to the value determined through dynamic light scattering (Galantai et al. 2000).

For analyzing the interaction between liposomes and HSA in the presence of MP, we then mixed liposome preparations of both lipid compositions (DMPC and DMPC/DMPG) with a HSA–MP solution at the concentrations given in Table 3. FCS data were then taken

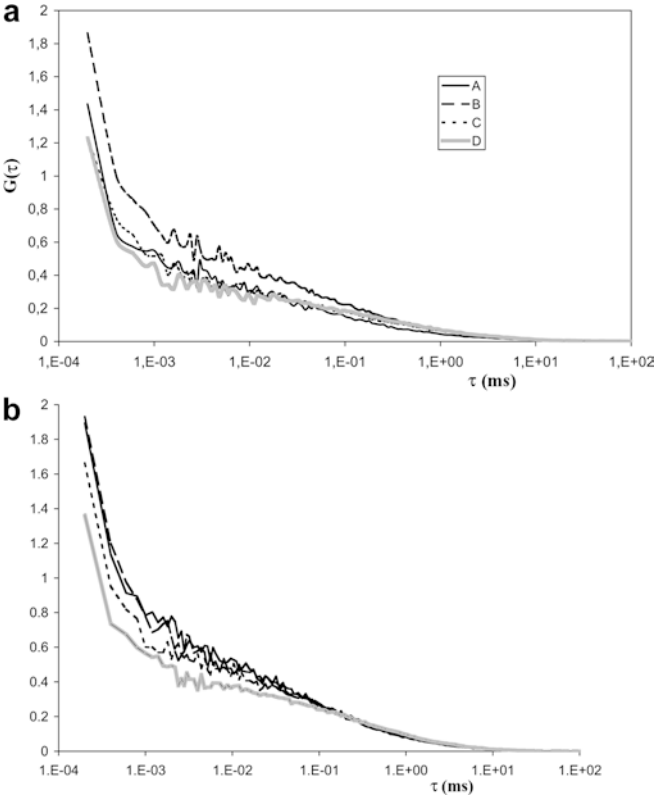

Fig. 4 FCS autocorrelation functions of (**a**) DMPC–liposome–HSA–MP and (**b**) DMPC/DMPG–liposome–HSA–MP solutions. Curves *A*, *B*, *C*, *D* represent the different concentrations that are given in Table 3

of these samples; typical autocorrelation functions are shown in Fig. 4. For these data, usually three discrete components were needed to obtain a satisfactory fit, although in some cases two were sufficient. In Table 4 we only show the τ_{diff} parameter corresponding to the main liposome component.

MEM analysis applied to the same data gave the diffusion time distributions shown in Fig. 5. Table 5 shows the corresponding diffusion constants and hydrodynamic radii obtained from the median values of the peaks.

Comparing the results from the discrete-component fit with the MEM analysis, we see a clear concentration dependence of the liposome diffusion time obtained in the discrete analysis: for the higher lipid concentrations, τ_{diff} increases. MEM, on the other hand, gives a stable value for the diffusion time of the liposome component that shows no trend with changing concentration. We suppose that the reason for this difference lies in the fact that the actual diffusion time distributions exhibit rather broad features, which makes a discrete analysis more uncertain and will artificially shift values of one fitted component when the amplitude of another one changes, as is the case here. We have one sharper peak around 1 ms that

Table 4 Average τ_{diff} values for DMPC and DMPC/DMPG liposomes at 32 °C as determined from a discrete-component fit. Values are the average from two independent samples at different lipid concentrations as given in Table 3

	DMPC τ_{diff} (ms)	DMPC/DMPG τ_{diff} (ms)
A	0.36 ± 0.2	0.70 ± 0.04
B	0.56 ± 0.1	0.87 ± 0.04
C	0.92 ± 0.06	0.55 ± 0.16
D	1.05 ± 0.21	1.00 ± 0.14

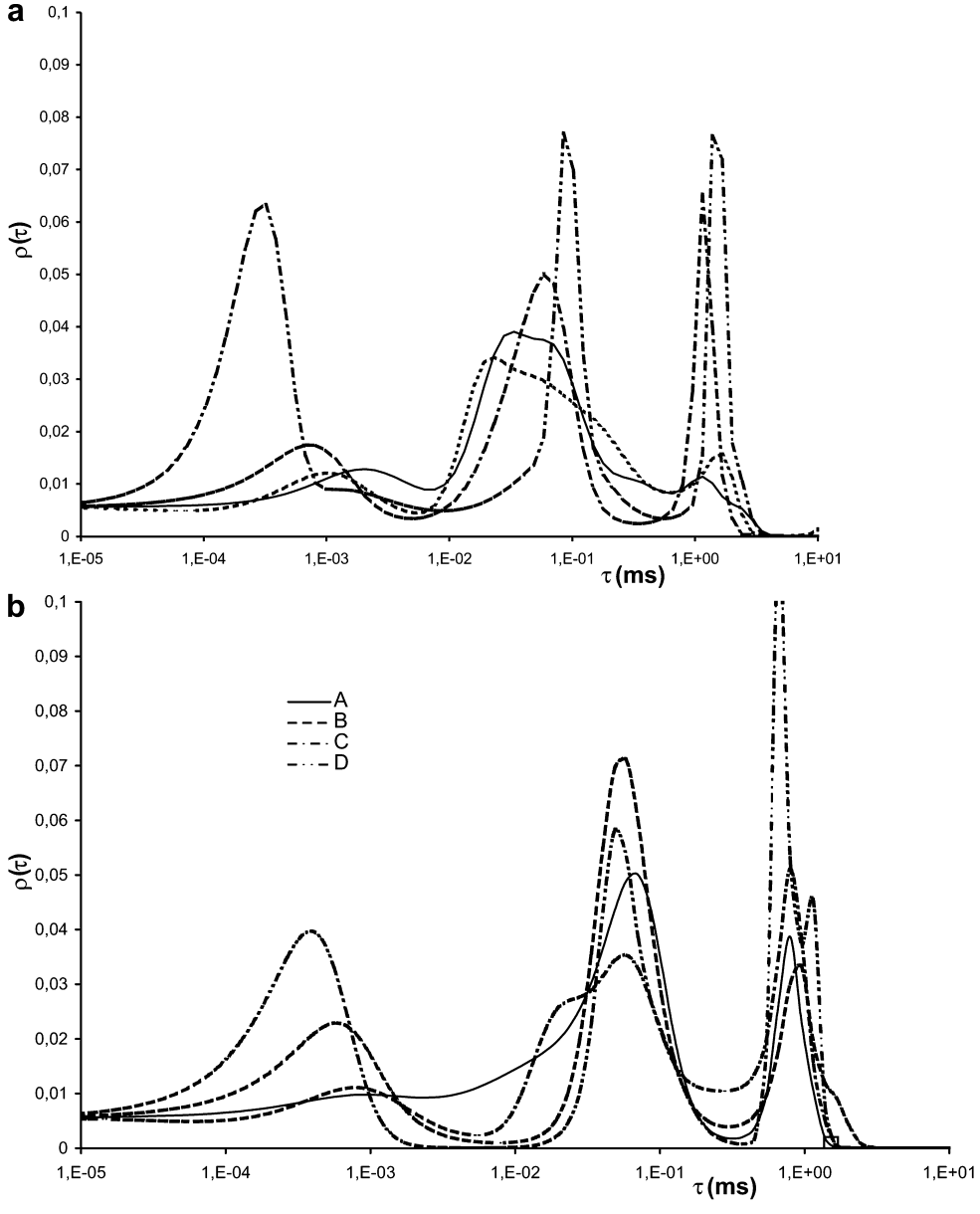

Fig. 5 Calculated diffusion time distributions values of mixtures of (**a**) HSA, MP, and DMPC, and (**b**) DMPC/DMPG liposomes characterized by their effective diffusion time (τ_{diff}). The graphs are the average over two measurements from independent samples

Table 5 Measured effective diffusion times at 32 °C, computed diffusion constants, and hydrodynamic radii for the liposome peak in the different mixtures of liposomes, HSA, and MP. A, B, C, and D correspond to the concentration values in Table 3

Sample	τ_{diff} (ms)	D_t (m^2 s^{-1})	r (nm)
DMPC (A)	1 ± 0.17	$(1.4 \pm 0.24) \times 10^{-11}$	21 ± 3.6
DMPC (B)	0.7 ± 0.26	$(2.1 \pm 0.8) \times 10^{-11}$	14 ± 5.2
DMPC (C)	0.97 ± 0.09	$(1.5 \pm 0.14) \times 10^{-11}$	19 ± 1.8
DMPC (D)	1 ± 0.15	$(1.4 \pm 0.21) \times 10^{-11}$	21 ± 3.2
DMPC/DMPG (A)	0.79 ± 0.15	$(1.8 \pm 0.34) \times 10^{-11}$	16 ± 3
DMPC/DMPG (B)	0.95 ± 0.06	$(1.5 \pm 0.1) \times 10^{-11}$	19 ± 1.2
DMPC/DMPG (C)	0.75 ± 0.12	$(1.9 \pm 0.3) \times 10^{-11}$	15 ± 2.4
DMPC/DMPG (D)	0.81 ± 0.08	$(1.7 \times \pm 0.17) \times 10^{-11}$	17 ± 1.7

Table 6 Relative area under the HSA and liposome peaks in Fig. 5

	A	B	C	D
DMPC/HSA				
Peak 2 (HSA)	0.810	0.774	0.707	0.621
Peak 3 (liposomes)	0.190	0.226	0.293	0.379
DMPC-DMPG/HSA				
Peak 2 (HSA)	0.802	0.749	0.670	0.537
Peak 3 (liposomes)	0.198	0.251	0.330	0.463

corresponds to the liposome and another wide peak around 0.1 ms that is related to the diffusion of free HSA.

From the peak areas in Fig. 5 we can then characterize the relative contributions of the HSA and liposome components to the FCS data. The peak at fast diffusion times corresponds to the error in the estimate of the triplet amplitude and relaxation rate, which in this version of the FCS program has to be done beforehand through a discrete-component fit (as described above). That peak, therefore, was not included in the calculation. The relative areas of the two peaks corresponding to HSA and liposomes are shown in Table 6; we clearly see that the increasing lipid concentration from A to D is reflected in the relative contribution of the liposome peak. However, in all samples a substantial amount of HSA is still detected.

It is worth noting that the observation of liposomes in a system containing the HSA–MP complex and unlabelled liposomes is in good agreement with our previous results that showed the binding of HSA to this SUV (Galantai and Bardos-Nagy 2000; Galantai et al. 2000; Bardos-Nagy et al. 2003). The fact that the liposome signal increases with increasing amount of lipid concentrations indicates that the amount of HSA–liposome complex increases, so the saturation condition is not fulfilled at the applied HSA/lipid concentration ratios. Again, the Stokes' radius of the liposomes is similar to the value from dynamic light scattering (Galantai et al. 2000).

In summary, we conclude that FCS data from a heterogeneous system like the one studied here can be analyzed more stably using the MEM method than with a discrete fitting algorithm. A further improvement of the method is possible by including discrete non-fluorescent terms into the parameters, which will be implemented in a future version of the program.

A Windows-executable version of the MEM program (written in Borland Delphi/Pascal) is available upon request from the authors.

References

Bárdos-Nagy I, Galantai R, Kaposi A, Fidy J (1998) Difference in the transport of metal and free-base porphyrins. Steady-state and time-resolved fluorescence studies. Int J Pharm 175:255–267

Bardos-Nagy I, Galantai R, Laberge M, Fidy J (2003) The effect of trehalose on the nonbond associative interactions between small unilamellar vesicles and human serum albumin and on the aging process. Langmuir 19:146–153

Bryan R (1990) Maximum entropy analysis of oversampled data problems. Eur Biophys J 18:165

Chen Y, Müller JD, Tetin SY, Tyner JD, Gratton E (2000) Probing ligand protein binding equilibria with fluorescence fluctuation spectroscopy. Biophys J 79:1074–1084

Elson EL, Magde D (1974) Fluorescence correlation spectroscopy. I. Conceptual basis and theory. Biopolymers 13:1–27

Ferrer ML, Duchowicz R, Carrasco B, de la Torre, JG, Acuna AU (2001) The conformation of serum albumin in solution: a combined phosphorescence depolarization-hydrodynamic modeling study. Biophys J 80:2422–2430

Galantai R, Bardos-Nagy I (2000) The interaction of human serum albumin and model membranes. Int J Pharm 195:207–18

Galantai R, Bardos-Nagy I, Modos K, Kardos J, Zavodszky P, Fidy J (2000) Serum albumin-lipid membrane interaction influencing the uptake of porphyrins. Arch Biochem Biophys 373:261–270

Gull SF, Daniell GJ (1978) Image reconstruction from incomplete and noisy data. Nature 272:686–690

Langowski J, Bryan R (1991) Maximum entropy analysis of photon correlation spectroscopy data using a Bayesian estimate for the regularization parameter. Macromolecules 24:6346–6348

Langowski J, Tewes M (2000) Determination of DNA-ligand interactions by fluorescence correlation spectroscopy. In: Travers A, Buckle M (eds) Protein-DNA interactions: a practical approach. Oxford University Press, Oxford, pp 95–111

Magde D, Elson EL, Webb WW (1972) Thermodynamic fluctuations in a reacting system—measurement by fluorescence correlations spectroscopy. Phys Rev Lett 29:705–708

Magde D, Elson EL, Webb WW (1974) Fluorescence correlation spectroscopy. II. An experimental realization. Biopolymers 13:29–61

Oncley JL, Scatchard G, Brown A (1947) Physical-chemical characteristics of certain of the proteins of normal human plasma. J Phys Colloid Chem 51:184

Press WH, Flannery BP, Teukolsky SA, Vetterling VT (1986) Numerical recipes in C: the art of scientific computing. Cambridge University Press, Cambridge

Qian H, Elson EL (1991) Analysis of confocal laser-microscope optics for 3-D fluorescence correlation spectroscopy. Appl Opt 30:1185–1195

Reddi E, Ricchelli F, Jori G (1981) Interaction of human serum albumin with hematoporphyrin and its Zn(2)+- and Fe(3)+-derivatives. Int J Pept Protein Res 18:402–408

Rigler R, Mets Ü, Widengren J, Kask P (1993) Fluorescence correlation spectroscopy with high count rate and low background: analysis of translational diffusion. Eur Biophys J 22:169–175

Rouser G, Simon G, Kritchevsky G (1969) Species variations in phospholipid class distribution of organs. I. Kidney, liver and spleen. Lipids 4:599–606

Skilling J, Bryan RK (1984) Maximum entropy image reconstruction: general algorithm. Mon Not R Astron Soc 211:111–124

Widengren J, Mets Ü, Rigler R (1995) Fluorescence correlation spectroscopy of triplet states in solution: a theoretical and experimental study. J Phys Chem 99:13368–13379